



*Supplement of*

## **Life–cycle impacts of South Korean air pollution on tropospheric ozone and methane: sensitivity to dispersion time**

**Calum Patrick Wilson and Michael John Prather**

*Correspondence to:* Calum Patrick Wilson ([calumw@uci.edu](mailto:calumw@uci.edu))

The copyright of individual parts of the supplement might differ from the article licence.

## Supplement: Life–Cycle Impacts of South Korean Air Pollution on Tropospheric Ozone and Methane: Sensitivity to Dispersion Time

### Contents

#### S1. Emission temporal profiles

**Figure S1:** Days of the week (left) and hours of the day (right) temporal scale factors for EDGAR v4.3.2 emissions for the month of May.

**Table S1:** Total South Korean emission rates and reactivity lifetimes used to derive our emission temporal scale factors.

#### S2. BL-RL model vertical levels

**Table S2:** The ERA5 vertical coordinates used in the BL-RL model stage.

#### S3. Model-observation comparison

**Table S3:** Model vs. observation performance metrics in the South Korean boundary layer (BL).

**Figure S2:** Mean diurnal cycles of surface observations (black lines) and model output (Coloured lines) for O<sub>3</sub> (top), CO (middle), and NO<sub>x</sub> (bottom).

**Figure S3:** Surface Observation and BL-RL model statistics for O<sub>3</sub> (blue), CO (red), and NO<sub>x</sub> (green).

**Figure S4:** Mean daytime O<sub>3</sub> concentration in the model (top) and gridded observations (bottom).

**Figure S5:** Mean daytime CO concentration in the model (top) and gridded observations (bottom).

**Figure S6:** Mean daytime NO<sub>x</sub> concentration in the model (top) and gridded observations (bottom).

**Figure S7:** Map of DC-8 observations in the BL (left) and FT (right) coloured by NO<sub>y</sub>-nitrogen (top) and VOC-carbon (bottom) mole fraction.

### Supplement references

## S1. Emission temporal profiles

Our temporal distributions for emissions profiles are derived using sectoral-resolved emissions from EDGAR v4.3.2 and separate temporal profiles (Crippa *et al.*, 2020). They are resolved diurnally (every hour), by day-of-the-week (weekday, Saturday, and Sunday), and by month for the following emission sectors: agricultural waste burning, energy for buildings, fugitive emissions from refining, fuel exploitation, off-road transport, road transport, power generation, and combustion for manufacturing (see Figure S1). Our derived temporal profiles are a linear combination of the EDGAR sector-specific temporal profiles, and are applied equally to all KORUS v5 emissions (Woo *et al.*, 2020) in each grid-cell.

In each model grid-cell, we estimate a single, fractional contribution of the eight emission sectors to the grid-cell emissions; these weightings are used to average the EDGAR temporal profiles over the sectors. The sector contributions are computed as the EDGAR sector-to-total emission ratio ( $\text{kg m}^{-2} \text{s}^{-1}$ ) summed over the inventoried air pollutants ( $\text{NO}_x$ , CO, and 25 VOCs; see Table S1 for totals), but with the emission densities weighted by the approximate inverse lifetimes of the species in the BL. The reactivity weightings ensure our calculated diurnal emission cycles represent the sectors in proportion to their influence on the BL-RL model chemistry.

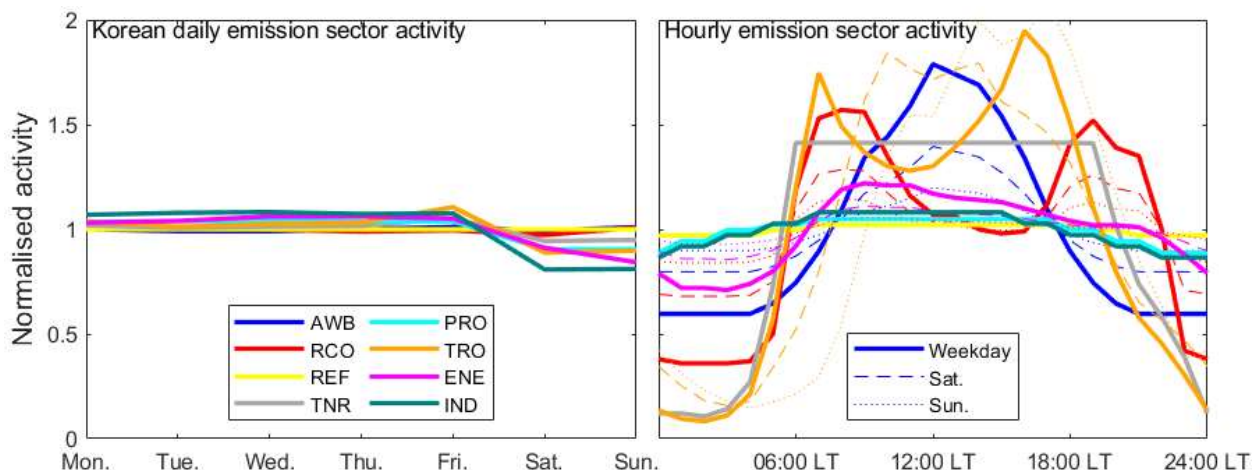


**Figure S1: Days of the week (left) and hours of the day (right) temporal scale factors for EDGAR v4.3.2 emissions for the month of May.** The sectors are denoted as follows: AWB (agricultural waste burning), RCO (energy for buildings), REF (fugitive emissions from refining), TNR (off-road transport, i.e., rail, shipping, aircraft landing & take-off), PRO (fuel exploitation), TRO (road transportation), ENE (power generation), and IND (combustion for manufacturing). Solid, dashed, and dotted lines in the hourly profiles (right) indicate weekday, Saturday, and Sunday diurnal cycles respectively. Local time for all cells is Korean Standard Time.

**Table S1: Total South Korean emission rates and reactivity lifetimes used to derive our emission temporal scale factors.**

| Emitted Species (SAPRC ID)    | EDGAR ID        | KORUS v5 flux (kg hr <sup>-1</sup> ) | EDGAR flux (kg hr <sup>-1</sup> ) | Lifetime (hr) | 1-hr decay fraction |       |
|-------------------------------|-----------------|--------------------------------------|-----------------------------------|---------------|---------------------|-------|
| CO                            | CO              | 20200                                | 33200                             | 2100          | 0.000               |       |
| NO                            | NO <sub>x</sub> | 85300                                | 143000                            | 6.0           | 0.154               |       |
| NO <sub>2</sub>               |                 | 17900                                |                                   |               |                     |       |
| Ethane (ALK1)                 | VOC02           | 3400                                 | 1400                              | 3000          | 0.000               |       |
| Propane (ALK2)                | VOC03           | 3900                                 | 8440                              | 560           | 0.002               |       |
| <i>n</i> -Butane (ALK3)       | VOC04           | 5300                                 | 5300                              | 250           | 0.004               |       |
| <i>n</i> -Pentane (ALK4)      | VOC05           | 65000                                | 22000                             | 719           | 140                 | 0.007 |
| <i>n</i> -Hexane (ALK4)       | VOC06           |                                      |                                   | 100           | 0.010               |       |
| <i>n</i> -Heptane (ALK5)      |                 |                                      |                                   | 80            | 0.012               |       |
| Ethene                        | VOC07           | 7690                                 | 3750                              | 43            | 0.023               |       |
| Propene (OLE1)                | VOC08           | 4100                                 | 1470                              | 9.0           | 0.105               |       |
| Isoprene                      | VOC10           | 650                                  | 16                                | 3.8           | 0.231               |       |
| Butadiene (OLE2)              | VOC12           | 5400                                 | 3520                              | 6.2           | 0.149               |       |
| Benzene (ARO1)                | VOC13           | 33000                                | 3170                              | 460           | 0.002               |       |
| Toluene (ARO1)                | VOC14           |                                      | 4710                              | 95            | 0.010               |       |
| <i>m</i> -Xylene (ARO2)       | VOC15           |                                      | 5560                              | 24            | 0.041               |       |
| 1,2,4-Trimethylbenzene (ARO2) | VOC16           |                                      | 17000                             | 564           | 17                  | 0.057 |
| Cresols                       | VOC17           |                                      | 100                               | 4590          | 12                  | 0.080 |
| HCHO                          | VOC21           | 990                                  | 308                               | 6.6           | 0.141               |       |
| Acetaldehyde                  | VOC22           | 560                                  | 564                               | 27            | 0.036               |       |
| Propionaldehyde (RCHO)        |                 | 300                                  |                                   | 13            | 0.074               |       |
| Methylglyoxal                 |                 | 90                                   |                                   | 2.1           | 0.379               |       |
| Benzaldehyde                  |                 | 30                                   |                                   | 33            | 0.030               |       |
| Diacetyl                      |                 | 30                                   |                                   | 1.0           | 0.632               |       |
| Acetone                       | VOC23           | 340                                  | 2560                              | 71            | 0.014               |       |
| Methyl ethyl ketone           |                 | 570                                  |                                   | 99            | 0.010               |       |

South Korean emissions from KORUS v5 and EDGAR v4.3.2 are shown as sums over the BL-RL model domain for the month of May. Named species in the model are represented by both explicit and lumped categories, e.g., “ALK1” in KORUS v5, and “VOC06” in EDGAR. KORUS v5 fluxes are converted from mol s<sup>-1</sup> to kg hr<sup>-1</sup> for comparison with EDGAR using the masses of the representative “emitted species” in our modelling system. EDGAR emission fluxes were

*partitioned into sectors, scaled by the 1-hr decay fractions, then used as weightings to estimate the sector activity fraction in each terrestrial BL-RL grid-cell. The reactivity scalings are computed from OH rate constants in MCM v3.3.1 (Bloss et al., 2005; Jenkin et al., 1997; Jenkin et al., 2003; Jenkin et al., 2015; Saunders et al., 2003) using  $[OH] = 5 \times 10^5$  molec  $cm^{-3}$  and temperature = 288 K. In each grid-cell, the sector activities are used as weightings to average the sector-based temporal profiles shown in Figure S1.*

## S2. BL-RL model vertical levels

**Table S2: The ERA5 vertical coordinates used in the BL-RL model stage.**

| ERA5 level index (l) | Lower edge-level quantities |          |         |       | Mid-level quantities |       |                |  |
|----------------------|-----------------------------|----------|---------|-------|----------------------|-------|----------------|--|
|                      | $\eta_A$ (Pa)               | $\eta_B$ | p (hPa) | z (m) | $\delta p$ (hPa)     | T (K) | $\delta z$ (m) |  |
| 99                   | 16262                       | 0.411    | 574     | 4566  | NA                   | NA    | NA             |  |
| 100                  | 15597                       | 0.438    | 594     | 4287  | 20.6                 | 268.9 | 278            |  |
| 101                  | 14898                       | 0.466    | 615     | 4017  | 20.6                 | 270.4 | 270            |  |
| 102                  | 14173                       | 0.494    | 636     | 3755  | 20.5                 | 271.8 | 262            |  |
| 103                  | 13428                       | 0.522    | 656     | 3503  | 20.4                 | 273.2 | 253            |  |
| 104                  | 12668                       | 0.549    | 676     | 3260  | 20.1                 | 274.5 | 243            |  |
| 105                  | 11901                       | 0.577    | 696     | 3028  | 19.7                 | 275.7 | 232            |  |
| 106                  | 11133                       | 0.604    | 715     | 2806  | 19.3                 | 276.9 | 222            |  |
| 107                  | 10370                       | 0.630    | 734     | 2595  | 18.8                 | 278.0 | 211            |  |
| 108                  | 9618                        | 0.656    | 752     | 2394  | 18.2                 | 279.0 | 200            |  |
| 109                  | 8880                        | 0.681    | 769     | 2205  | 17.5                 | 280.0 | 189            |  |
| 110                  | 8163                        | 0.705    | 786     | 2026  | 16.9                 | 280.9 | 179            |  |
| 111                  | 7470                        | 0.728    | 802     | 1858  | 16.1                 | 281.8 | 168            |  |
| 112                  | 6804                        | 0.750    | 818     | 1701  | 15.4                 | 282.7 | 158            |  |
| 113                  | 6169                        | 0.771    | 832     | 1553  | 14.6                 | 283.5 | 148            |  |
| 114                  | 5564                        | 0.791    | 846     | 1415  | 13.9                 | 284.3 | 138            |  |
| 115                  | 4994                        | 0.810    | 859     | 1286  | 13.1                 | 285.1 | 129            |  |
| 116                  | 4457                        | 0.827    | 872     | 1167  | 12.4                 | 285.8 | 120            |  |
| 117                  | 3956                        | 0.844    | 883     | 1055  | 11.6                 | 286.4 | 111            |  |
| 118                  | 3489                        | 0.859    | 894     | 952   | 10.9                 | 287.1 | 103            |  |
| 119                  | 3057                        | 0.874    | 905     | 856   | 10.2                 | 287.6 | 96             |  |
| 120                  | 2659                        | 0.887    | 914     | 768   | 9.5                  | 288.2 | 88             |  |
| 121                  | 2294                        | 0.900    | 923     | 686   | 8.8                  | 288.7 | 82             |  |
| 122                  | 1962                        | 0.911    | 931     | 611   | 8.2                  | 289.1 | 75             |  |
| 123                  | 1659                        | 0.922    | 939     | 541   | 7.6                  | 289.5 | 69             |  |
| 124                  | 1388                        | 0.932    | 946     | 478   | 7.1                  | 289.9 | 64             |  |
| 125                  | 1143                        | 0.941    | 952     | 419   | 6.5                  | 290.2 | 59             |  |
| 126                  | 926.5                       | 0.949    | 958     | 365   | 6.0                  | 290.5 | 54             |  |
| 127                  | 735.0                       | 0.957    | 964     | 315   | 5.6                  | 290.7 | 50             |  |
| 128                  | 568.1                       | 0.963    | 969     | 270   | 5.1                  | 290.9 | 45             |  |
| 129                  | 424.4                       | 0.970    | 974     | 228   | 4.7                  | 291.1 | 42             |  |
| 130                  | 302.5                       | 0.975    | 978     | 190   | 4.3                  | 291.2 | 38             |  |
| 131                  | 202.5                       | 0.980    | 982     | 155   | 4.0                  | 291.4 | 35             |  |
| 132                  | 122.1                       | 0.985    | 986     | 123   | 3.7                  | 291.6 | 32             |  |
| 133                  | 62.8                        | 0.989    | 989     | 94    | 3.4                  | 291.7 | 29             |  |
| 134                  | 22.8                        | 0.992    | 992     | 67    | 3.1                  | 291.9 | 27             |  |
| 135                  | 3.76                        | 0.995    | 995     | 43    | 2.8                  | 292.0 | 24             |  |
| 136                  | 0.000                       | 0.998    | 998     | 20    | 2.6                  | 292.0 | 22             |  |
| 137                  | 0.000                       | 1.000    | 1000    | 0     | 2.4                  | 292.0 | 20             |  |

*ERA5 levels index mid-level meteorological variables (e.g.  $T$  and  $q$ ; Hersbach et al., 2025) and lower-edge pressure levels ( $p$ ) defined by hybrid parameters  $\eta_A$  and  $\eta_B$ , for a surface pressure of 1000 hPa. Layer thicknesses ( $\delta z$ ) are computed from the hydrostatic equation using pressure thicknesses ( $dp$ ),  $T$ , and  $q$  (not shown), then integrated from the surface to obtain the lower-edge heights ( $z$ ).*

### S3. Model-observation comparison

Table S2 and Figures S2-S6 compare O<sub>3</sub>, CO, and NO<sub>x</sub> mole fractions in the “boundary layer-residual layer” (BL-RL) modelling stage, resolved as mixed BL column values, with NIER surface site data gridded to model resolution (0.1°x0.1°, hourly). Our comparisons are decomposed into four time periods characterised according to meteorology by Peterson et al., 2019: dynamic (01-16 May), anticyclone (17-22 May), transport (25-31 May), and rex-block (01-07 June). Figure S7 shows the geography of NASA DC-8 sampling during the KORUS-AQ mission, as used for model-observation comparison in the “plume” (PL) modelling stage.

**Table S3: Model vs. observation performance metrics in the South Korean boundary layer (BL).**

| Meteorological Phase  | Mean daytime bias (ppb) | Correlation (Pearson-r) | Model daytime max (ppb) | Obs. daytime max (ppb) | Model daytime min (ppb) | Obs. daytime min (ppb) |
|-----------------------|-------------------------|-------------------------|-------------------------|------------------------|-------------------------|------------------------|
| <b>O<sub>3</sub></b>  |                         |                         |                         |                        |                         |                        |
| Dynamic               | 21.6                    | 0.58                    | 79.5                    | 64.3                   | 59.5                    | 32.1                   |
| Anticyclone           | -0.8                    | 0.78                    | 87.1                    | 95.8                   | 51.0                    | 52.0                   |
| Transport             | -1.4                    | 0.75                    | 98.9                    | 101.2                  | 48.2                    | 47.5                   |
| Rex block             | 21.6                    | 0.74                    | 111.0                   | 83.2                   | 61.5                    | 39.0                   |
| <b>CO</b>             |                         |                         |                         |                        |                         |                        |
| Dynamic               | -136.8                  | 0.35                    | 232.8                   | 571.7                  | 114.1                   | 132.9                  |
| Anticyclone           | -126.3                  | 0.26                    | 623.1                   | 799.4                  | 119.2                   | 151.1                  |
| Transport             | -236.4                  | 0.28                    | 525.5                   | 808.4                  | 117.3                   | 194.6                  |
| Rex block             | -123.7                  | 0.30                    | 449.2                   | 692.4                  | 115.3                   | 123.8                  |
| <b>NO<sub>x</sub></b> |                         |                         |                         |                        |                         |                        |
| Dynamic               | -16.7                   | 0.54                    | 41.8                    | 45.3                   | 0.5                     | 10.1                   |
| Anticyclone           | -9.4                    | 0.50                    | 89.5                    | 57.6                   | 1.5                     | 10.6                   |
| Transport             | -9.7                    | 0.53                    | 93.9                    | 57.5                   | 1.6                     | 11.9                   |
| Rex block             | -12.5                   | 0.51                    | 71.8                    | 51.5                   | 1.3                     | 9.0                    |

Model data are BL column values from the BL-RL model. Data were sampled in grid-cells observed by at least five effective NIER sites, during the full days defined by the meteorological

phases (see text in Section 4). Pearson's correlation coefficients were computed over the full diurnal cycles while mean daytime bias (model minus observation), daytime max, and daytime min columns were sampled during the period from 13:00-17:00 LT. Daytime maxes and mins were computed on individual days during the phases, then averaged over those meteorological stages.

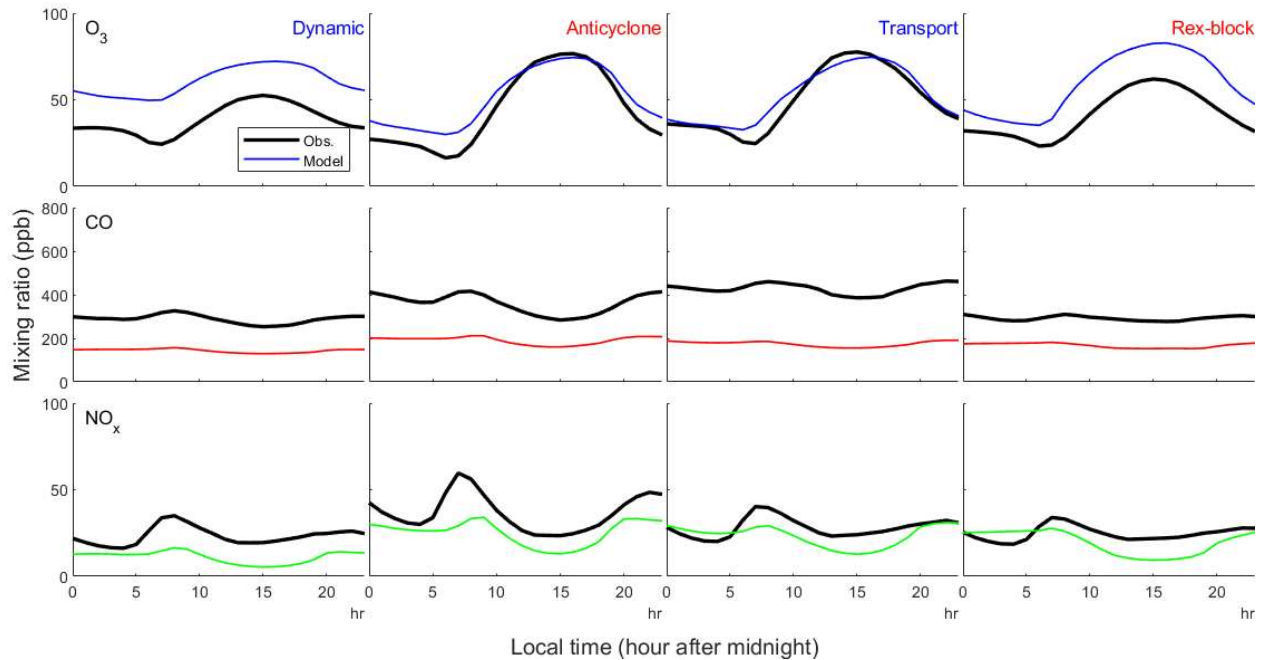


**Figure S2: Mean diurnal cycles of surface observations (black lines) and model output (Coloured lines) for O<sub>3</sub> (top), CO (middle), and NO<sub>x</sub> (bottom).** All data were sampled in grid-cells observed by at least five effective NIER sites. Diurnal averages were sampled separately within the meteorological stages as described in Peterson et al. (2019).

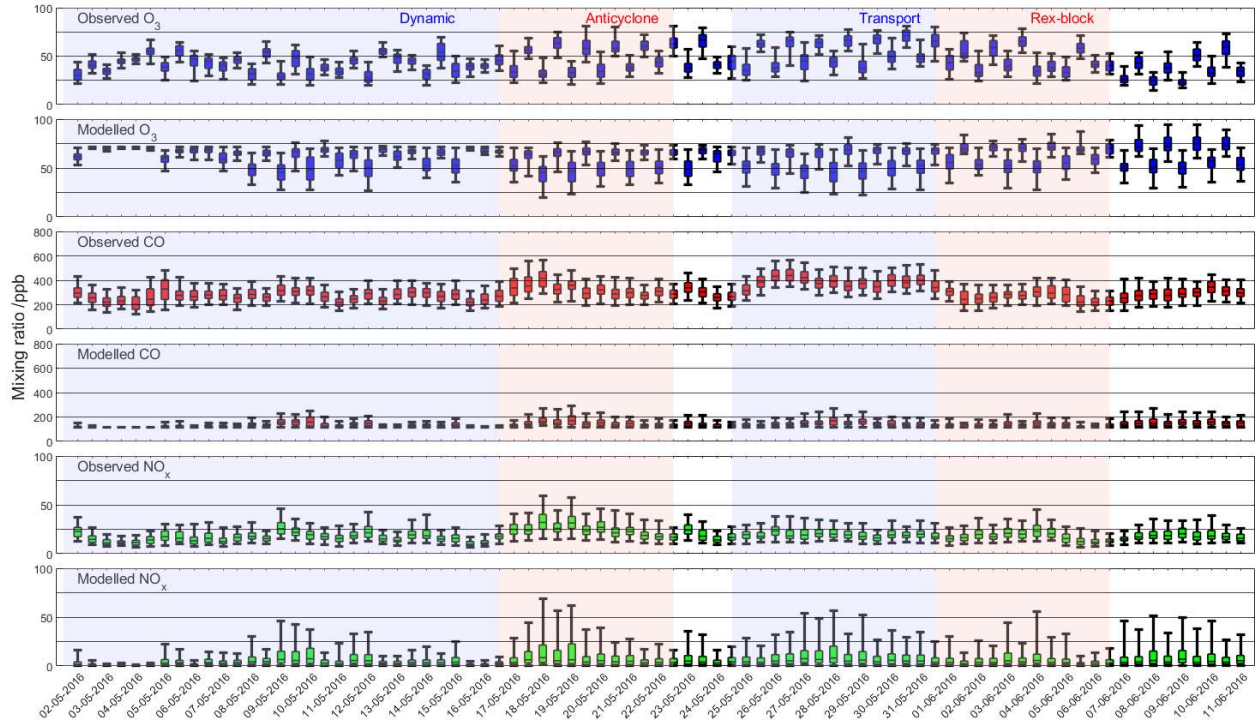


**Figure S3: Surface Observation and BL-RL model statistics for O<sub>3</sub> (blue), CO (red), and NO<sub>x</sub> (green).** Boxes represent the medians, quartiles, 5<sup>th</sup>, and 95<sup>th</sup> percentiles of ozone observations (top) and model output (bottom), where observations were interpolated to the model grid (see Wilson and Prather, 2025). Data were averaged over twelve-hourly intervals between 06:00 and 18:00, and the meteorological stages described by Peterson et al. (2019) are highlighted by blue and red shading.

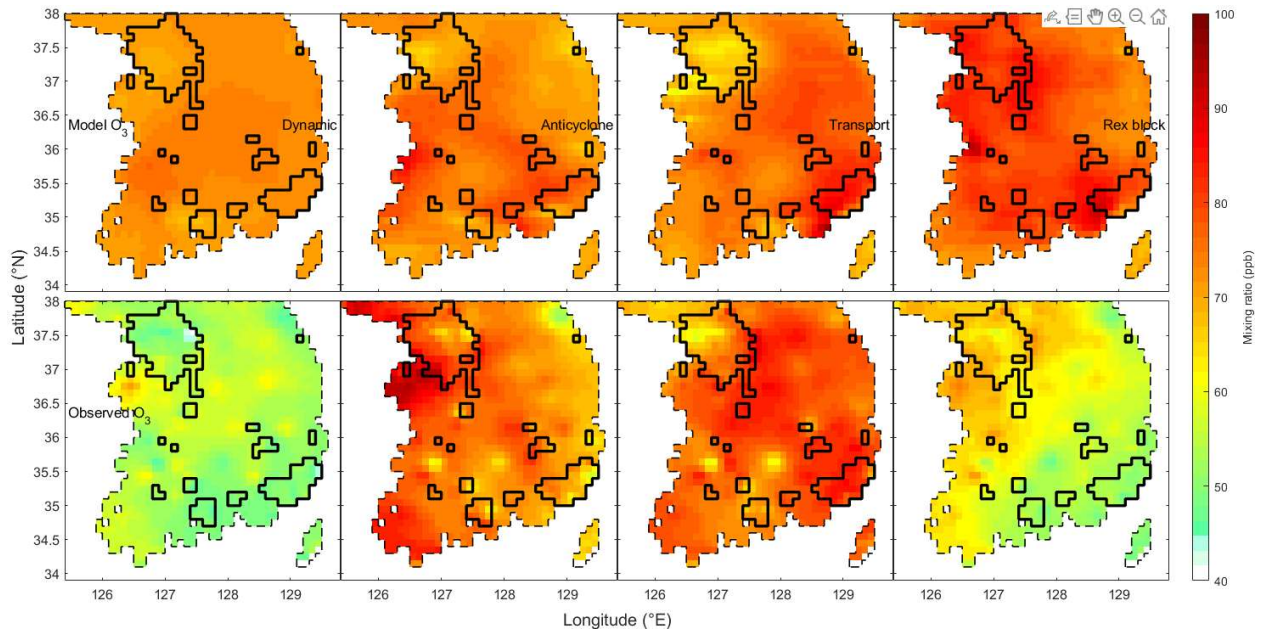


**Figure S4: Mean daytime  $O_3$  concentration in the model (top) and gridded observations (bottom).** Grid-cell means were computed between 13:00 and 18:00 during the four meteorological phases (left-to-right): 01-16 May (dynamic), 17-22 May (anticyclone), 25-31 May (transport), and 01-07 June (rex-block). Bold lines enclose grid-cells that were effectively observed by at least five NIER sites during the KORUS-AQ period. Dashed lines enclose the BL-RL model domain

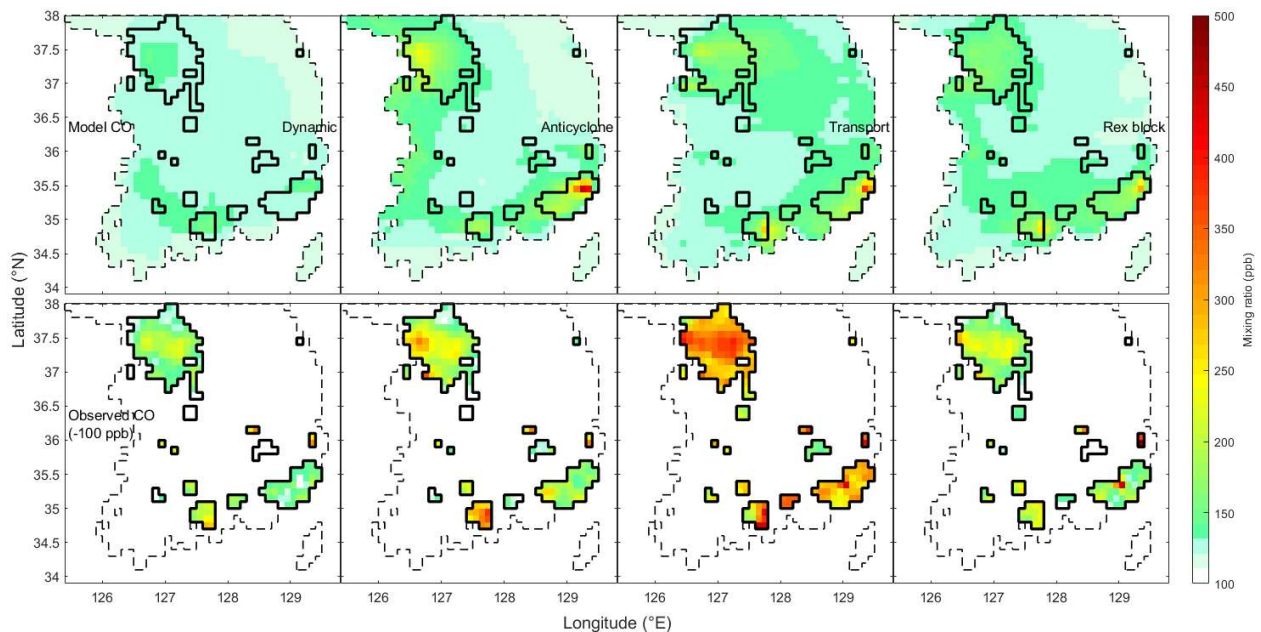


**Figure S5: Mean daytime  $CO$  concentration in the model (top) and gridded observations (bottom).** As in Figure S4, but for  $CO$ . Gridded observations produced from fewer than five effective NIER sites are not shown, and a 100 ppb correction has been subtracted from the observations to better represent DC-8 boundary layer observations (Wilson and Prather, 2025).

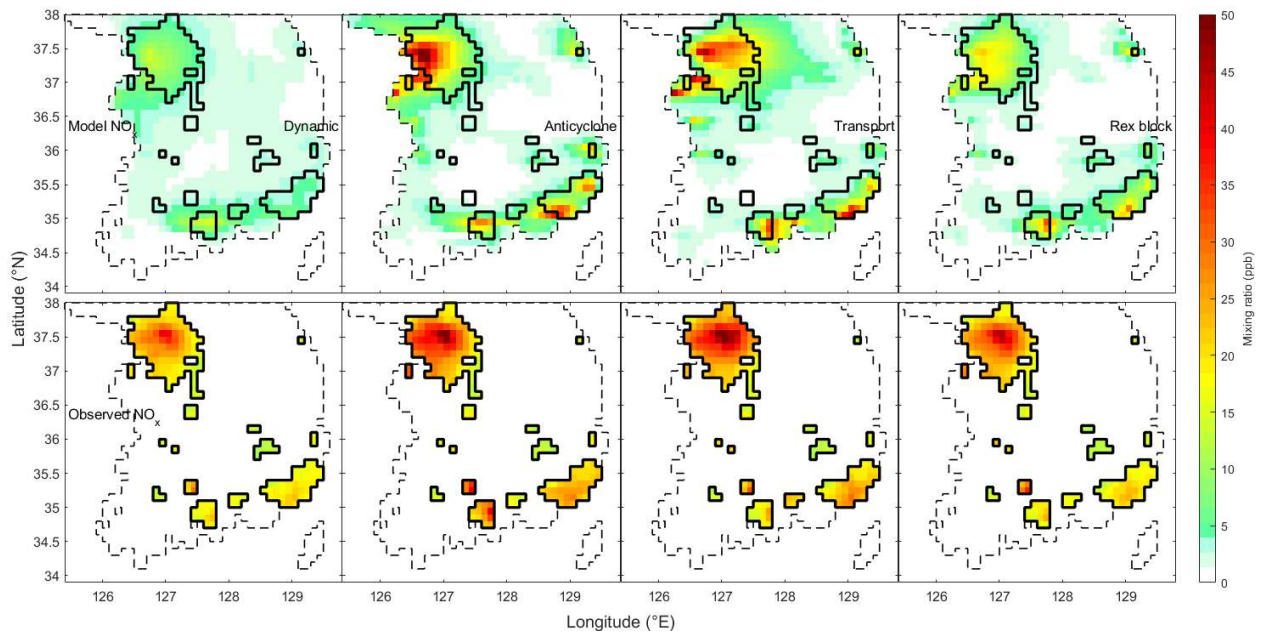


**Figure S6: Mean daytime NO<sub>x</sub> concentration in the model (top) and gridded observations (bottom).** As in Figure S4, but for NO<sub>x</sub>. Gridded observations produced from fewer than five effective NIER sites are not shown.

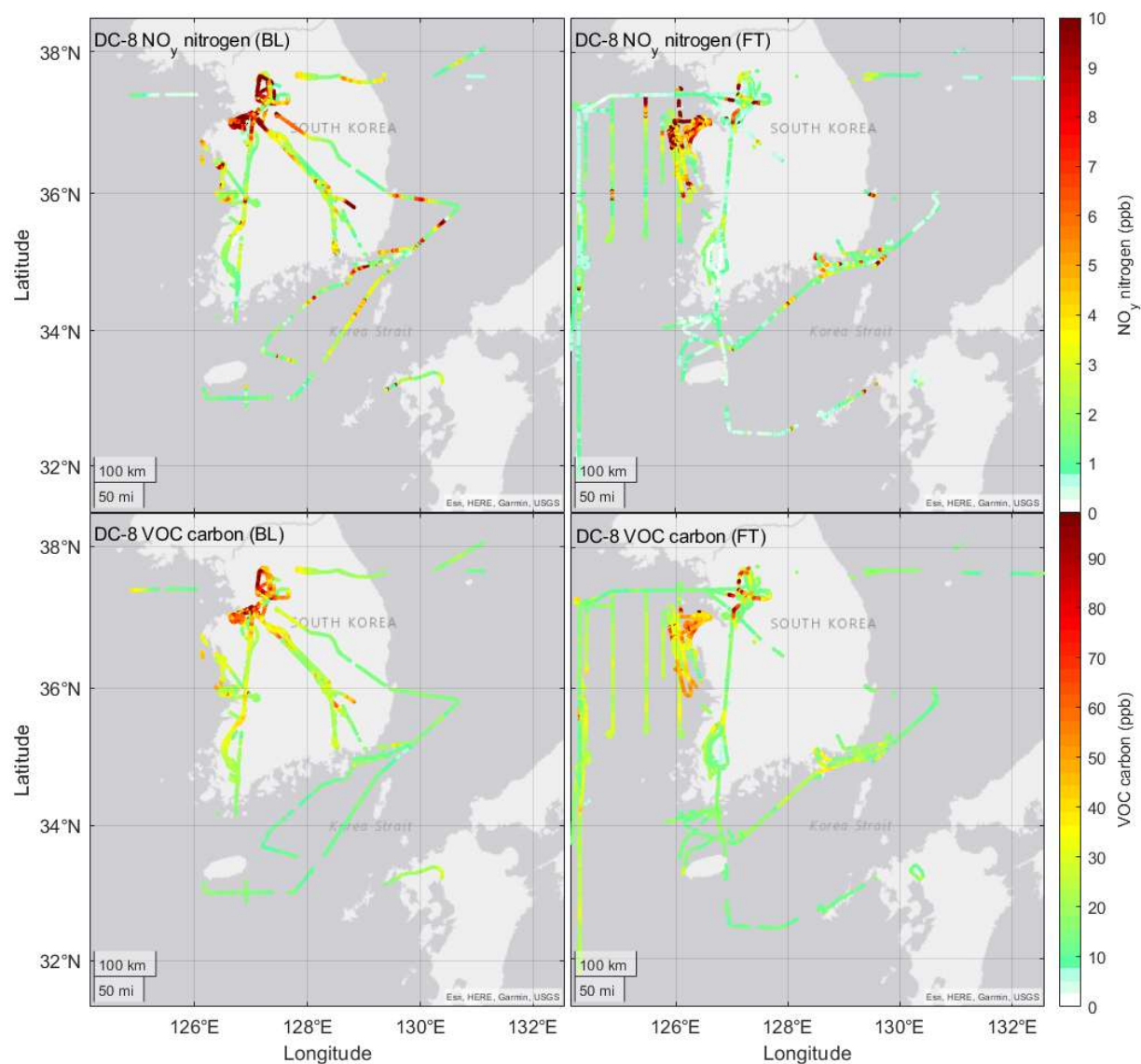


**Figure S7: Map of DC-8 observations in the BL (left) and FT (right) coloured by  $\text{NO}_y$ -nitrogen (top) and VOC-carbon (bottom) mole fraction.** Flight segments (coloured circles) are 10 s merges of 1 Hz KORUS data (KORUS-AQ Science Team, 2019), sampled above (left) and below (right) the hourly,  $0.25^\circ \times 0.25^\circ$  ERA5 BL height (Hersbach et al., 2023).  $\text{NO}_y$  includes  $\text{NO}$  and  $\text{NO}_2$  measured by the NCAR four-channel chemiluminescence instrument (Weinheimer et al., 1993) with PAN and PPN from the Georgia Tech Chemical Ionization Mass Spectrometer (GT-CIMS; Huey, 2007). For carbon, VOCs include ethane, benzene, toluene, isoprene, methacrolein, acetaldehyde, acetone, methyl ethyl ketone, and methyl vinyl ketone by Proton Transfer Reaction Mass Spectrometry (PTR-MS; Müller et al., 2014) and formaldehyde by the Compact Atmospheric Multispecies Spectrometer (CAMS; Richter et al., 2015; Spinei et al., 2018). Esri, HERE, Garmin, USGS | Powered by Esri.

## Supplement references

Bloss, C.; Wagner, V.; Jenkin, M. E.; Volkamer, R.; Bloss, W. J.; Lee, J. D.; Heard, D. E.; Wirtz, K.; Martin-Reviejo, M.; Rea, G.; Wenger, J. C.; Pilling, M. J. Development of a Detailed Chemical Mechanism (MCMv3.1) for the Atmospheric Oxidation of Aromatic Hydrocarbons. *Atmospheric Chemistry and Physics* 2005, 5 (3), 641–664. <https://doi.org/10.5194/acp-5-641-2005>.

Crippa, M.; Solazzo, E.; Huang, G.; Guizzardi, D.; Koffi, E.; Muntean, M.; Schieberle, C.; Friedrich, R.; Janssens-Maenhout, G. High Resolution Temporal Profiles in the Emissions Database for Global Atmospheric Research. *Sci Data* 2020, 7 (1), 121. <https://doi.org/10.1038/s41597-020-0462-2>.

Hersbach, H., Bell, B., Berrisford, P., Biavati, G., Horányi, A., Muñoz Sabater, J., Nicolas, J., Peubey, C., Radu, R., Rozum, I., Schepers, D., Simmons, A., Soci, C., Dee, D., Thépaut, J.-N. (2023): ERA5 hourly data on single levels from 1940 to present. Copernicus Climate Change Service (C3S) Climate Data Store (CDS), DOI: 10.24381/cds.adbb2d47 (Accessed on 26-Feb-2025)

Huey, L. G. Measurement of Trace Atmospheric Species by Chemical Ionization Mass Spectrometry: Speciation of Reactive Nitrogen and Future Directions. *Mass Spectrometry Reviews* 2007, 26 (2), 166–184. <https://doi.org/10.1002/mas.20118>.

Jenkin, M. E.; Saunders, S. M.; Pilling, M. J. The Tropospheric Degradation of Volatile Organic Compounds: A Protocol for Mechanism Development. *Atmospheric Environment* 1997, 31 (1), 81–104. [https://doi.org/10.1016/S1352-2310\(96\)00105-7](https://doi.org/10.1016/S1352-2310(96)00105-7).

Jenkin, M. E.; Saunders, S. M.; Wagner, V.; Pilling, M. J. Protocol for the Development of the Master Chemical Mechanism, MCM v3 (Part B): Tropospheric Degradation of Aromatic Volatile Organic Compounds. *Atmospheric Chemistry and Physics* 2003, 3 (1), 181–193. <https://doi.org/10.5194/acp-3-181-2003>.

Jenkin, M. E.; Young, J. C.; Rickard, A. R. The MCM v3.3.1 Degradation Scheme for Isoprene. *Atmospheric Chemistry and Physics* 2015, 15 (20), 11433–11459. <https://doi.org/10.5194/acp-15-11433-2015>.

KORUS-AQ Science Team: KORUS-AQ NASA DC-8 airborne 10 s merged data revision 6 - ICARTT Files, NASA Langley Atmospheric Science Data Center DAAC [data set], <https://doi.org/10.5067/Suborbital/KORUSAQ/DATA01>, 2019.

Müller, M.; Mikoviny, T.; Feil, S.; Haidacher, S.; Hanel, G.; Hartungen, E.; Jordan, A.; Märk, L.; Mutschlechner, P.; Schottkowsky, R.; Sulzer, P.; Crawford, J. H.; Wisthaler, A. A Compact PTR-ToF-MS Instrument for Airborne Measurements of Volatile Organic Compounds at High Spatiotemporal Resolution. *Atmospheric Measurement Techniques* 2014, 7 (11), 3763–3772. <https://doi.org/10.5194/amt-7-3763-2014>.

Peterson, D. A.; Hyer, E. J.; Han, S.-O.; Crawford, J. H.; Park, R. J.; Holz, R.; Kuehn, R. E.; Eloranta, E.; Knute, C.; Jordan, C. E.; Lefer, B. L. Meteorology Influencing Springtime Air Quality, Pollution Transport, and Visibility in Korea. *Elementa: Science of the Anthropocene* 2019, 7, 57. <https://doi.org/10.1525/elementa.395>.

Richter, D.; Weibring, P.; Walega, J. G.; Fried, A.; Spuler, S. M.; Taubman, M. S. Compact Highly Sensitive Multi-Species Airborne Mid-IR Spectrometer. *Appl. Phys. B* 2015, 119 (1), 119–131. <https://doi.org/10.1007/s00340-015-6038-8>.

Saunders, S. M.; Jenkin, M. E.; Derwent, R. G.; Pilling, M. J. Protocol for the Development of the Master Chemical Mechanism, MCM v3 (Part A): Tropospheric Degradation of Non-Aromatic Volatile Organic Compounds. *Atmospheric Chemistry and Physics* 2003, 3 (1), 161–180. <https://doi.org/10.5194/acp-3-161-2003>.

Spinei, E.; Whitehill, A.; Fried, A.; Tiefengraber, M.; Knepp, T. N.; Herndon, S.; Herman, J. R.; Müller, M.; Abuhassan, N.; Cede, A.; Richter, D.; Walega, J.; Crawford, J.; Szykman, J.; Valin, L.; Williams, D. J.; Long, R.; Swap, R. J.; Lee, Y.; Nowak, N.; Poche, B. The First Evaluation of Formaldehyde Column Observations by Improved Pandora Spectrometers during the KORUS-AQ Field Study. *Atmospheric Measurement Techniques* 2018, 11 (9), 4943–4961. <https://doi.org/10.5194/amt-11-4943-2018>.

Weinheimer, A. J., Walega, J. G., Ridley, B. A., Sachse, G. W., Anderson, B. E., & Collins Jr., J. E. Stratospheric NO<sub>y</sub> measurements on the NASA DC-8 during AASE II. *Geophysical Research Letters* 1993, 20 (22), 2563–2566. <https://doi.org/10.1029/93GL02627>

Wilson, C. P.; Prather, M. J. Gridded Surface O<sub>3</sub>, NO<sub>x</sub>, and CO Abundances for Model Metrics from the South Korean Ground Station Network. *Atmospheric Measurement Techniques* 2025, 18 (8), 1757–1769. <https://doi.org/10.5194/amt-18-1757-2025>.

Woo, J.-H.; Kim, Y.; Kim, H.-K.; Choi, K.-C.; Eum, J.-H.; Lee, J.-B.; Lim, J.-H.; Kim, J.; Seong, M. Development of the CREATE Inventory in Support of Integrated Climate and Air Quality Modeling for Asia. *Sustainability* 2020, 12 (19), 7930. <https://doi.org/10.3390/su12197930>.